Detection of metastatic tumors after γ-irradiation using longitudinal molecular imaging and gene expression profiling of metastatic tumor nodules

SU JIN JANG[1,2], JOO HYUN KANG[1], YONG JIN LEE[1], KWANG IL KIM[1], TAE SUP LEE[1], JAE GOL CHOE[2] and SANG MOO LIM[1]

[1]Molecular Imaging Research Center, Korea Institute of Radiological and Medical Sciences (KIRAMS), Seoul 139-706, [2]Department of Nuclear Medicine, Korea University Anam Hospital, Korea University College of Medicine, Seoul 136-705, Republic of Korea

Received December 8, 2015; Accepted January 11, 2016

DOI: 10.3892/ijo.2016.3384

Abstract. A few recent reports have indicated that metastatic growth of several human cancer cells could be promoted by radiotherapy. C6-L cells expressing the firefly luciferase (fLuc) gene were implanted subcutaneously into the right thigh of BALB/c nu/nu mice. C6-L xenograft mice were treated locally with 50-Gy γ-irradiation (γ-IR) in five 10-Gy fractions. Metastatic tumors were evaluated after γ-IR by imaging techniques. Total RNA from non-irradiated primary tumor (NRPT), γ-irradiated primary tumor (RPT), and three metastatic lung nodule was isolated and analyzed by microarray. Metastatic lung nodules were detected by BLI and PET/CT after 6-9 weeks of γ-IR in 6 (17.1%) of the 35 mice. The images clearly demonstrated high [^{18}F]FLT and [^{18}F]FDG uptake into metastatic lung nodules. Whole mRNA expression patterns were analyzed by microarray to elucidate the changes among NRPT, RPT and metastatic lung nodules after γ-IR. In particular, expression changes in the cancer stem cell markers were highly significant in RPT. We observed the metastatic tumors after γ-IR in a tumor-bearing animal model using molecular imaging methods and analyzed the gene expression profile to elucidate genetic changes after γ-IR.

Correspondence to: Dr Joo Hyun Kang, Molecular Imaging Research Center, Korea Institute of Radiological and Medical Sciences (KIRAMS), 75 Nowon-gil, Gongneung-Dong, Nowon-Gu, Seoul 139-706, Republic of Korea
E-mail: kang2325@kirams.re.kr

Dr Jae Gol Choe, Department of Nuclear Medicine, Korea University Anam Hospital, Korea University College of Medicine, 126-1, 5 ga, Anam-dong, Seongbuk-gu, Seoul 136-705, Republic of Korea
E-mail: choejg@korea.ac.kr

Key words: γ-irradiation, metastatic tumors, molecular imaging, gene expression profiling, aldehyde dehydrogenases

Introduction

Glioma is the most common malignant primary brain tumor; thus, it is treated aggressively with surgery and chemotherapy and radiotherapy. The poor survival of patients with glioma reflects the prevalence of cancer recurrence after surgery, invasion into other sites, and intrinsic or acquired resistance to chemotherapy and radiotherapy (1). Ionizing irradiation (IR) is the most commonly employed treatment modality for various human cancers and regional cancer disease. IR is often used in combined treatments with chemotherapy and surgery (2). Concomitant combination therapy is used to treat patients with non-small lung, head and neck, cervical cancer, and glioblastoma (3-7), ~50% of cancer patients receive radiotherapy (8). The goal of radiotherapy is to provide a suitable dose to the primary tumor, while minimizing IR side-effects to surrounding normal tissues. Notably, one of the problems with lower dose (0.1-0.6 Gy) or high dose (10 Gy and higher) fractionated radiotherapy is radio-resistance and bystander factors released among treated cancer cells and in an animal model (9). Patients undergoing radiotherapy for local tumor control show better survival rates than patients with radiation-induced secondary tumors, which is attributed primarily to the observation that local treatment failure increases the probability of developing metastatic disease at distant organ sites (10,11). The first study on the effect of local tumor IR on metastatic frequency in a transplantable mouse carcinoma model was reported in 1949 by Kaplan and Murphy (12). Since then, various research groups have reported that the incidence of metastasis increases after IR of the primary tumor (13). Radio-therapeutic effects are considered because of the induction of DNA damage causing cell cycle arrest, apoptosis and senescence (14). IR induces modifications in the tumor microenvironment, which have a profound impact on tumor biology (15) and the incurred tumor hypoxic conditions can promote metastasis by recurrence in untreated hypoxic cells (16). It is now becoming evident that IR can also result in cancer cells acquiring a stemness state characterized by increased stemness gene expression and a cancer stem cell-like phenotype (17). Some studies indicate that irradiated tumors

contain a stemness population and that growth of distant metastasis is driven by cancer stem-like cells. Furthermore, several studies have shown that the epithelial-mesenchymal transition (EMT) has a crucial role in IR resistance of cancer cells (18). EMT was initially recognized as an important process during the morphogenesis of epithelial tissue in embryonic development, and is now shown to be one of the key steps promoting tumor metastasis. The EMT maintains cancer stemness and is induced by various factors. Several effectors, including transforming growth factor (TGF)-β, fibronectin (Fn1), metalloproteinases (MMPs), vimentin (Vim) and cadherin, mediate the EMT. Acquisition of stemness results in metastasis along with CD24, CD133, β-catenin, Oct-4 and Sox-2 expression in non-small cell lung cancer cells (19). Although the relationships between PI3K/Akt/mTOR signaling, EMT and cancer stem cells are known, the regulation mechanisms of metastasis in irradiated tumor are still unclear.

Regular follow-up examinations, such as imaging and tumor marker tests, may be required after radiotherapy to detect metastasis at an early stage. Therefore, many investigators utilize advance imaging techniques to monitor neoplastic progression to metastasis, such as bioluminescence imaging (BLI), computed tomography (CT) and positron emission tomography (PET) (20). These imaging modalities can evaluate progression, such as tumor growth, metabolism, or metastasis *in vivo*, in a longitudinal manner. A non-invasive imaging method is indispensable for detecting tumor lesions in an internal organ, such as the lungs, liver or brain, and diagnosing and determining the size of tumors in a preclinical animal model (21-24). Other ways to detect cancer involved in distance metastasis include immunohistochemical staining of *ex vivo* biopsies; however, these often lack reproducibility and accuracy (25).

In the present study, metastatic tumors in C6-L xenografted mice were studied after local treatment with fractionated γ-IR. To accurately detect the metastatic nodules after γ-IR, we observed the effect of γ-IR on distant metastatic tumor growth using different imaging modalities, such as BLI and PET/CT. A non-invasive longitudinal imaging study with repeated measurements of metastatic nodules after γ-IR indicated extensive colonization of C6-L cells in the lungs within 6 weeks after γ-IR. We also identified and described the molecular events occurring after γ-IR through gene expression profiling to elucidate genetic changes. We identified the differentially expressed genes between the γ-IR primary tumors vs. non-γ-IR primary tumors and metastatic lung nodules vs. γ-IR primary tumors using an Agilent Expression microarray contained ~30,003 Entrez Gene RNAs. In particular, we found known cancer stem cell markers and detected EMT among the differentially expressed genes.

Materials and methods

Cell culture. C6 rat glioma cells and C6-L infected cells containing the firefly luciferase (fLuc) gene in lentiviral vectors were used with selected blasticidin treatment (5 mg/ml), as previously described by Park *et al* (26).

Xenograft model and local Agilent Expression microarray-IR. BALB/c nu/nu mice (females, 5-6 weeks of age) were purchased from Orient Bio, Inc. (Seoul, Korea). C6-L cells ($5x10^5$/head) were implanted subcutaneously into the right thigh of mice. When the tumors reached ≥80 mm^3 (15 days after inoculation), we randomly assigned them to the C6-L γ-irradiated (γ-IR) and non-IR groups. C6-L tumor-bearing mice were treated locally with 50 Gy γ-IR in five 10-Gy fractions every day using a ^{60}Co γ-IR source (Theratrom 780; AECL, Ltd., Mississauga, ON, Canada; n=35), but not the control group (n=5). The mice were anesthetized with an intraperitoneal injection of a mixture of zolazepam/tiletamine (50 mg/kg; Zoletil 50®; Virbac, Magny-en-Vexin, France) and xylazine (10 mg/kg; Rompun®; Bayer Healthcare, Berlin, Germany) fixed on an acryl plate. All experiments with animals were carried out according to the guidelines for the care and the use of experimental animals and were approved by the Korea Institute of Radiological and Medical Sciences.

BLI acquisition. BLI was performed with a highly sensitive, optical CCD camera mounted in a light-tight specimen chamber (IVIS200; Xenogen, Alameda, CA, USA). Animals were given the firefly substrate D-luciferin potassium salt diluted to 2.5 mg/100 μl in saline. The mice were injected intraperitoneally with 100 μl of this D-luciferin solution and were anesthetized (2% isoflurane) for *in vivo* imaging. The mice were placed on the stage inside the light-tight camera box with continuous exposure to 0.5% isoflurane. Image acquisition time was 10 min. Bioluminescence signals were expressed in units of photons per cm^2 per second per steradian ($p/cm^2/s/sr$). Imaging and signal quantification were controlled by the acquisition and analysis software (Living Image v. 2.50; Xenogen).

PET/CT image acquisition. Mice were imaged using a small animal PET/CT system (INVEON™; Siemens Preclinical Solutions, Knoxville, TN, USA). [^{18}F] Fluordeoxyglucose (FDG) (7.4 MBq, 200 μCi) was injected via tail vein 1 h prior to PET/CT scanning. [^{18}F] fluorothymidine (FLT) (same dose) was injected 2 h prior. Mice were anesthetized using 2% isoflurane. PET and CT images were acquired using small animal PET/CT scanner. The mice were moved to the PET scanner on the same bed and scanned for 30 min after CT acquisition. Tissue radioactivity was expressed as the percentage of injected radioactivity dose per gram of tissue (%ID/g). Visualization and analyses of PET images were carried out using AsiPRO™ software (Siemens Preclinical Solutions). Radioactivity concentration in the local region was calculated from the PET images using maximum pixel values.

Evaluation of fLuc expression for reverse transcription-polymerase chain reaction (RT-PCR) analysis with tissue. Total RNA was isolated from metastatic tissue and used as a template to produce cDNA using SuperScript III First-Strand Synthesis for RT-PCR (Invitrogen, Carlsbad, CA, USA). The synthesized cDNA was amplified using Taq DNA polymerase (iNtRON Biotechnology, Inc., Daejeon, Korea) with the fLuc primer: forward, 5'-CGC CTT GAT TGA CAA GGA TGG-3', and reverse, 5'-GGC CTT TAT GAG GAT CTC TCT-3'. The forward rat GADPH primer was 5'-CAG TGC CAG CCT CGT CTC AT-3' and the reverse primer was 5'-AGG GGC CAT CCA CAG TCT TC-3'.

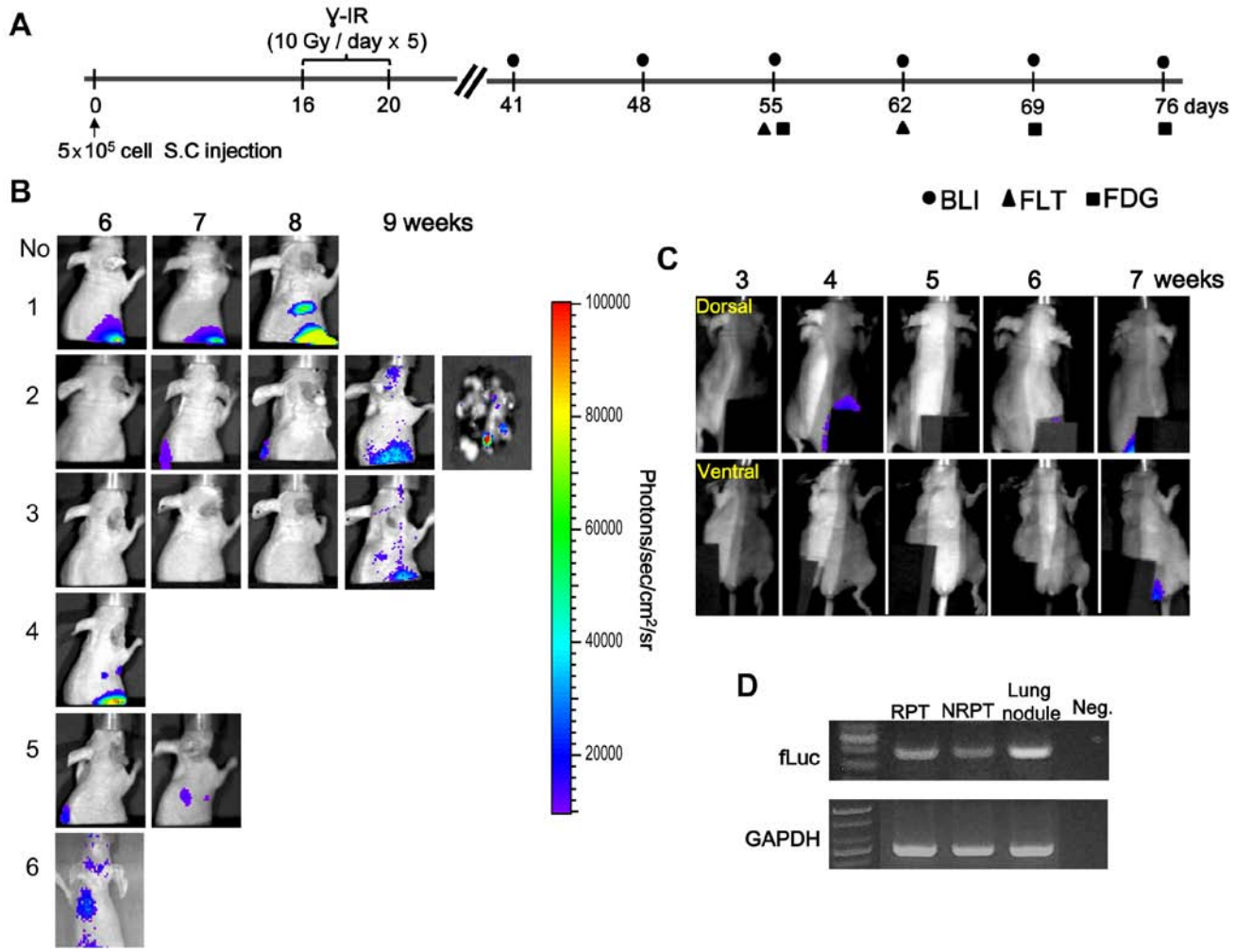

Figure 1. Detection of metastatic tumors after γ-IR by bioluminescence imaging (BLI). (A) Schedules of γ-IR treatment and image acquisition by BLI (●) and positron emission tomography/computed tomography with [^{18}F]FDG (■) and [^{18}F]FLT (▲). (B) Image was acquired from 3 weeks after γ-IR, we detected metastatic tumors in chest of No. 4 and 6 mice 6 weeks after γ-IR by BLI. No. 2 mouse was confirmed by *ex vivo*, hut the spot was not confirm on BLI. (C) BLI images of non-IR C6-L xenografted mice. After 3-7 weeks of xenograft, no distant metastasis was detected at a secondary site in the non-IR primary tumor model. (D) fLuc gene expression in metastatic lung nodules was confirmed by RT-PCR analysis using firefly luciferase and GAPDH specific primers (fLuc, 399 bp and rat GAPDH, 595 bp as an internal control).

Microarray analysis. Total RNA from primary tumors and IR-induced metastatic tissue for each model were used for expression profiling. Total RNA was purified using the Easy-spin Total RNA Extraction kit (iNtRON Biotechnology) according to the manufacturer's recommendations with the Agilent SurePrint G3 Rat Gene Expression 8x60K microarrays (Agilent Technologies, Inc., Santa Clara, CA, USA). The Agilent expression microarray contained ~30,003 Entrez Gene RNAs. The microarray analysis was done by Macrogen (Seoul, Korea). The arrays were scanned using the Agilent Technologies G2600D SG12494263. Array data export processing and analysis were performed using Agilent Feature Extraction software v11.0.1.1.

Results

Detection of metastatic tumors by BLI after γ-IR. The schedule for obtaining the BLI and nuclear medicine images beginning 4 weeks after γ-IR is presented in Fig. 1A. The BLI results of a longitudinal study of primary tumor growth and distant metastasis at a C6-L secondary site are shown in Fig. 1B and C. We detected metastatic tumors 6-9 weeks after γ-IR in the lungs by BLI and confirmed fLuc gene expression in the tissues (Fig. 1B and D). However, no distant metastasis was detected at the secondary site in the non-IR primary tumor (NRPT) model by BLI (Fig. 1C). Light emission of the lungs removed from sacrificed animal was examined at 9 weeks to confirm that the metastatic nodules were from the C6-L primary tumor (Fig. 1B, No. 2). This result suggests that the BLI signal from the lung originated from a γ-IR primary tumor (RPT) and was confirmed by RT-PCR (Fig. 1D). A fLuc-specific RT-PCR DNA band of 399 bp was detected in the metastatic lung nodules after γ-IR. However, survival of γ-IR treated mice was longer than that of the non-IR group because of the relatively low growth rate of the primary tumor mass after γ-IR (26).

Confirmation of metastatic tumor after γ-IR by nuclear medicine imaging. Metastatic nodules at secondary sites in the non-IR tumor model were monitored for 6 weeks by [^{18}F]FLT-PET (Fig. 2A), however, no metastatic nodules were

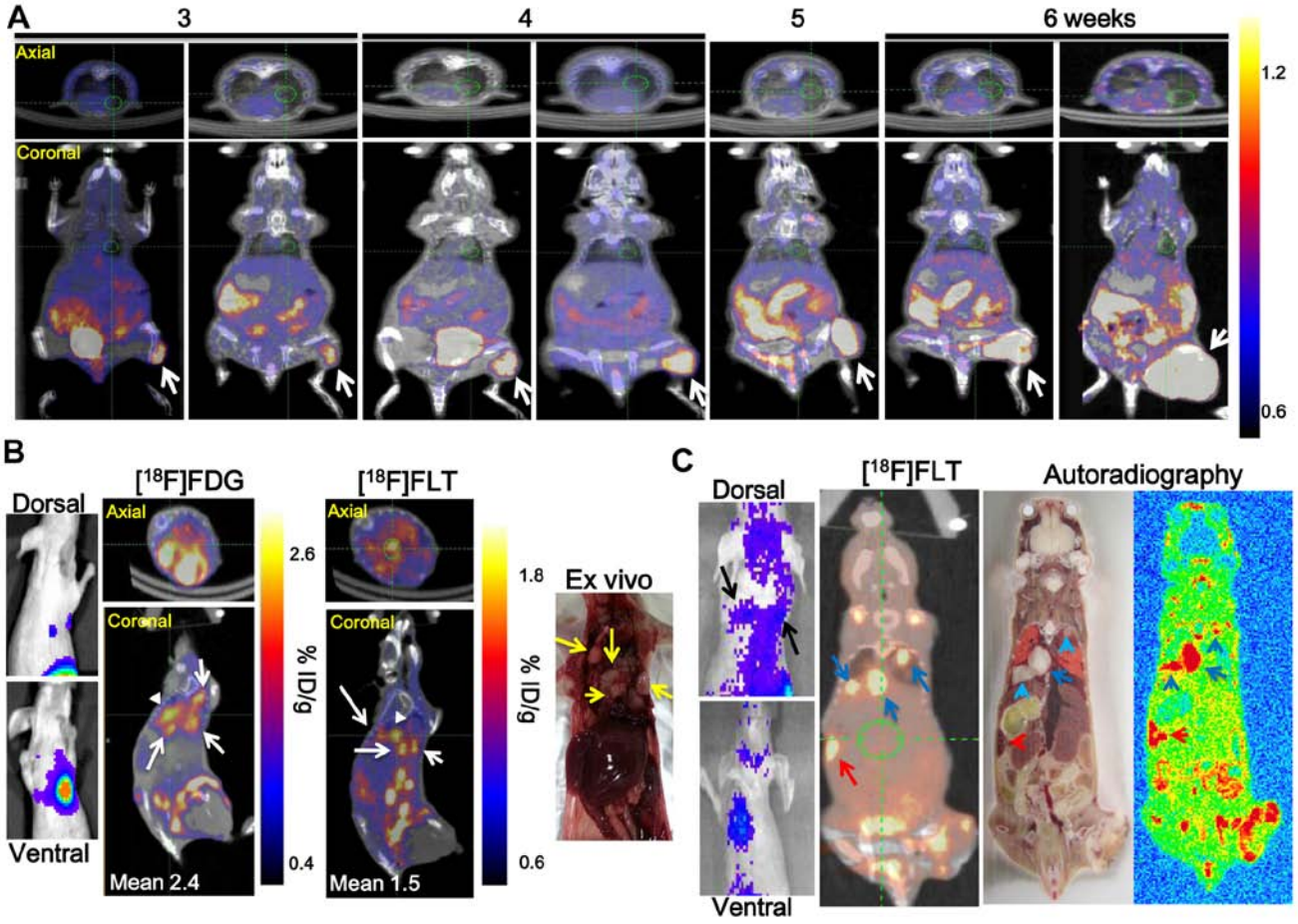

Figure 2. Confirmation of metastatic tumors after γ-irradiation (IR) by nuclear medicine imaging. The mice were imaged using positron emission tomography/computed tomography (PET/CT) 6 weeks after γ-IR using uptake of [^{18}F]FDG and [^{18}F]FLT. (A) The [^{18}F]FLT-PET image shows no metastatic nodules from non-IR primary tumor (NRPT) at a secondary site during 6 weeks. Arrows indicate the xenografted C6-L tumor. (B) BLI, [^{18}F]FDG and [^{18}F]FLT PET/CT of C6-L bearing mouse (No. 4 of Fig. 1B) 6 weeks after γ-IR. The images clearly demonstrate higher uptake of [^{18}F]FDG and [^{18}F]FLT in four metastatic lung nodules after γ-IR (white arrow). *Ex vivo* indication of macroscopic observation of nodules (yellow arrows) in lung. (C) BLI and [^{18}F]FLT PET/CT of C6-L bearing mouse (No. 6 of Fig. 1B) 6 weeks after γ-IR. [^{18}F]FLT PET/CT and autoradiography showed high [^{18}F]FLT uptake in metastatic nodules after γ-IR. Metastatic lung nodules were detected by [^{18}F]FLT and autoradiography (blue arrow), and other tissue metastasis were detected in the spleen (red arrow), but not by bioluminescence.

Table I. Summary of the incidence of metastatic nodules after γ-irradiation (IR).

No.	Images	Detection time (weeks)
1	WB BLI, nuclear imaging (FDG)	8
2	WB BLI, *ex vivo* BLI	9
3	WB BLI, nuclear imaging (FDG)	9
4	WB BLI, nuclear imaging (FDG, FLT), *ex vivo* BLI	6
5	WB BLI, nuclear imaging (FLT)	7
6[a]	WB BLI, nuclear imaging (FLT), autoradiography	6

WB, whole body; [a]microarray sample mouse.

detected at secondary sites. Mouse (No. 4 of Fig. 1B) underwent PET/CT 6 weeks after γ-IR and the administration of 7.4 MBq [^{18}F]FLT and [^{18}F]FDG to confirm the metastatic lung nodules after γ-IR detected by BLI via fLuc gene expression (Fig. 2B). [^{18}F]FLT and [^{18}F]FDG activity in the four metastatic lung nodules was high (Fig. 2B, white arrows). The activities were re-calculated using a region of interest analysis from a three-dimensional reconstruction encompassing the [^{18}F]FLT and [^{18}F]FDG uptake region. The [^{18}F]FLT and [^{18}F]FDG uptake values into one metastatic lung nodule was 1.5±0.13 and 2.4±0.24 %ID/g, respectively (white arrowhead). Three metastatic lung nodules (blue arrow) and one metastatic spleen nodule (red arrow) were detected by [^{18}F]FLT-PET and [^{18}F]FLT autoradiography in another γ-IR treated C6-L

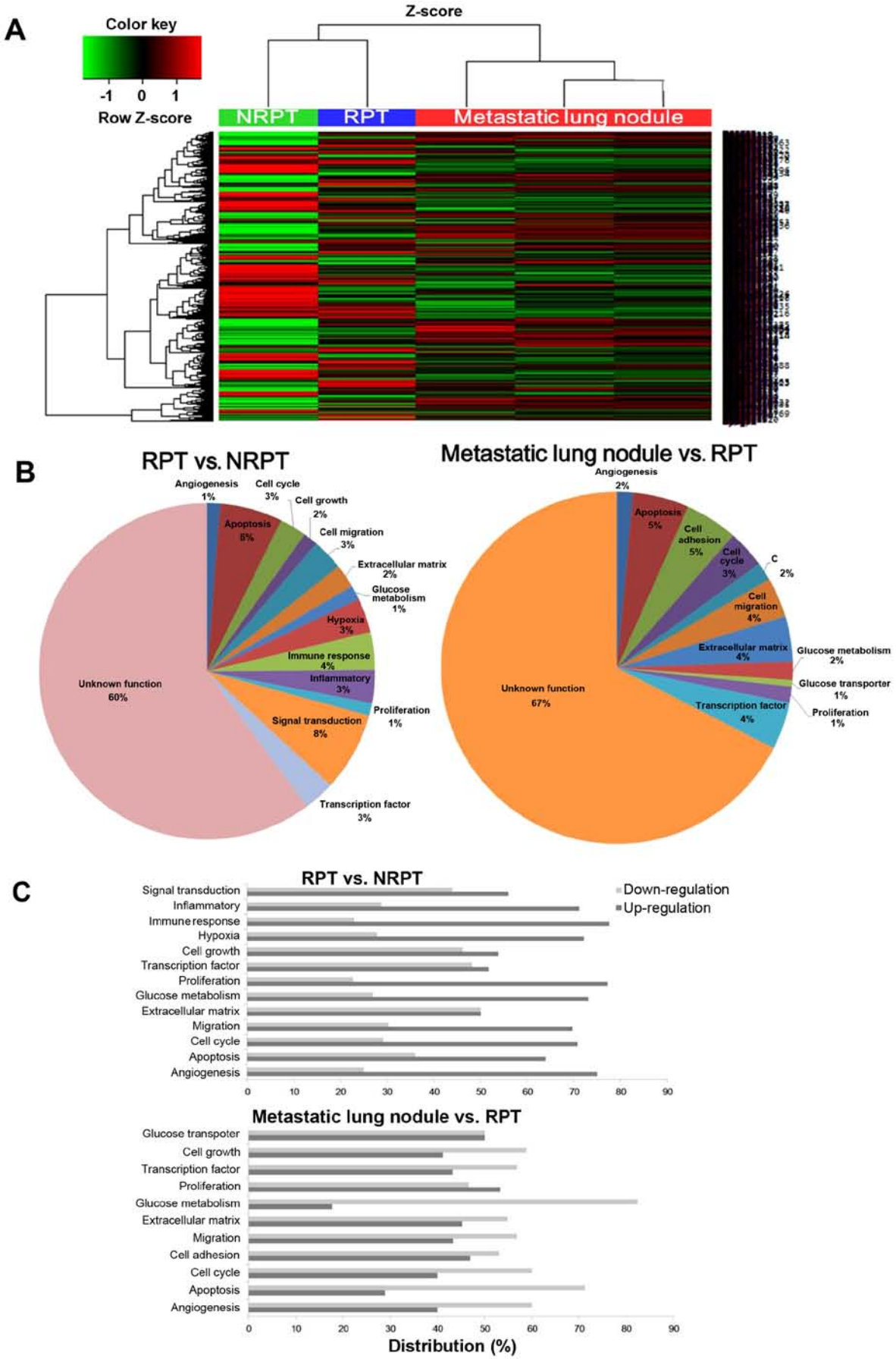

Figure 3. Comparison of primary and metastatic lung nodules. (A) Hierarchical clustering map of 3,881 differentially expressed genes in a non-irradiated (IR) primary tumor (NRPT), γ-IR treated C6-L primary tumor (RPT), and three metastatic lung nodules: red, upregulated; green, downregulated. The significance threshold was 2-fold with a P-value <0.05. (B) Pie chart shows different biological functional terms, (C) differential gene expression patterns based on categorization of the upregulated and downregulated genes. Comparisons between the RPT vs. NRPT and metastatic lung nodules vs. RPT categories were performed.

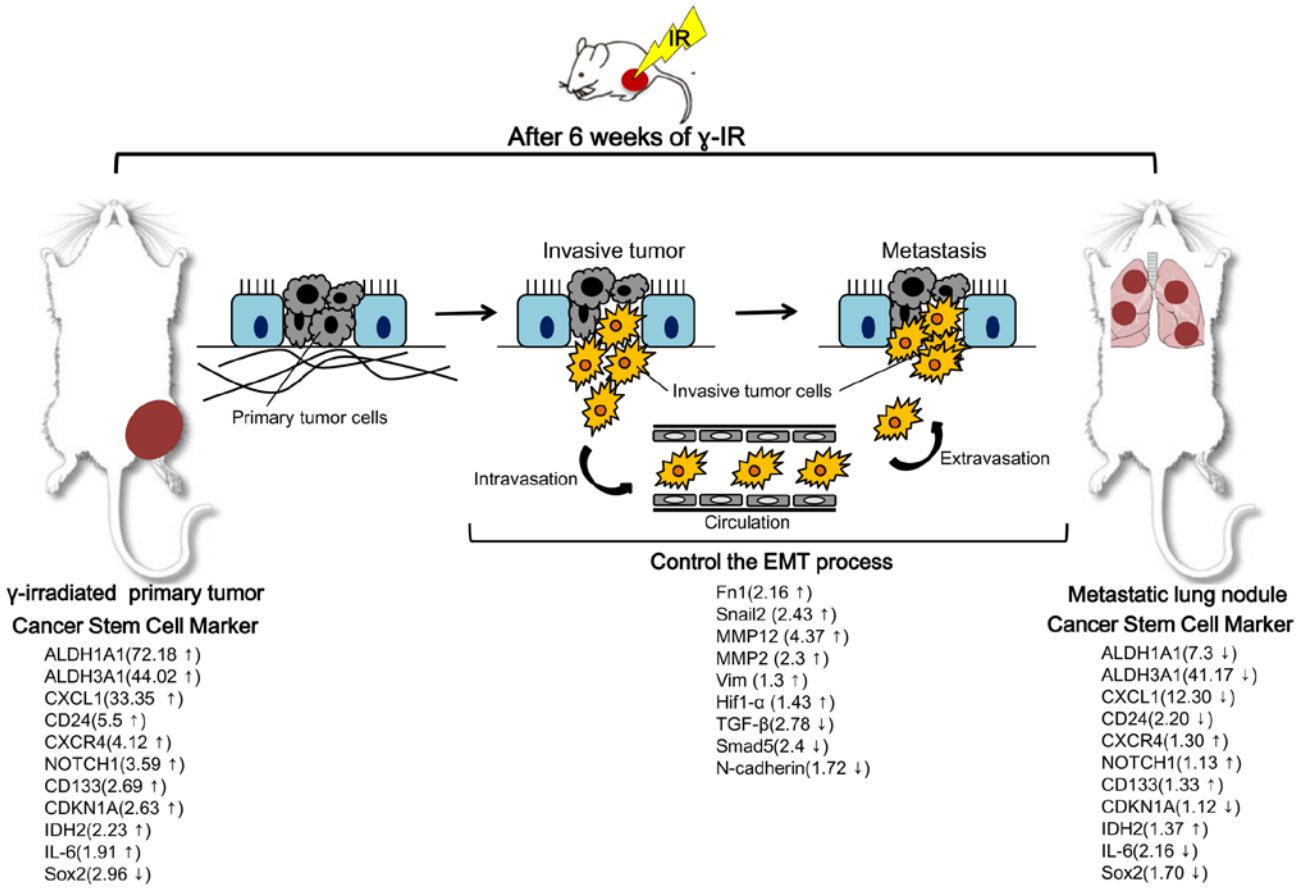

Figure 4. Diagram showing the model presented between the epithelial mesenchymal transition (EMT) and cancer stem cell marker in γ-irradiated (IR) C6-L primary tumor (RPT) and metastatic lung nodules after 6 weeks of γ-IR. Metastatic lung nodules after γ-IR with the EMT and enhanced cancer stem cell markers, resulting in C6-L metastasis and recurrence. However, the expression of cancer stem cell marker was downregulated in metastatic lung nodules after γ-IR.

bearing mouse (No. 6 of Figs. 1B and 2C). However, no splenic metastatic nodules were detected by BLI (Fig. 2C, left panel). Metastatic nodules were detected by BLI or nuclear medicine imaging in 6 (17.14%) of the 35 C6-L bearing mice from 6 weeks after γ-IR (Table I). RNA isolated from RPT, 3 metastatic lung nodules of mouse No. 6 of Fig. 1B, and NRPT of a non-irradiated mouse was analyzed by microarray.

Overview of metastatic tumors after γ-IR-related gene expression. The expression patterns of whole mRNAs were analyzed by microarray to elucidate the changes in NRPT, RPT and metastatic lung nodules. A hierarchical clustering analysis of 3,881 genes (≥2-fold change, P-value <0.05) indicated differentially expressed genes between the NRPT, RPT and three metastatic lung nodules (Fig. 3A). RPT and NRPT are closely clustered together and showed a similar heat map pattern of mRNA expression, which is different from that of the metastatic lung nodules. As shown in Fig. 3B, the biological process terms differ between the RPT vs. NRPT and the metastatic lung nodules vs. RPT that reflects their known functions. The RPT enriched genes have linked biological process terms: hypoxia (3%), immune response (4%), inflammatory (3%) and signal transduction (8%). In contrast, transcription factor (4%) and glucose metabolism (2%) are linked by biological process terms for the metastatic lung nodules. Gene Ontology (GO) analysis was performed using DAVID to gain a comprehensive understanding of the gene classes that were differentially regulated in the RPT vs. NRPT and the metastatic lung nodules vs. RPT (Fig. 3C). We found upregulated expression of angiogenesis, migration, and proliferation-related genes in RPT but downregulated expression in glucose metabolism-related genes and apoptosis in the metastatic lung nodules. The molecular mechanisms and therapeutic targets underlying metastatic tumors after γ-IR remain unclear. Identifying metastatic tumors using γ-IR-related molecular target will be helpful to identify useful therapeutic targets, developing novel treatment approaches, and overcome recurrence after γ-IR in patients with glioma. We present novel insight into the EMT and enhanced stemness in RPT based on our total gene expression analysis in γ-IR tumor tissue and metastatic lung nodules of the genes of interest. Our findings are summarized in Fig. 4. In particular, expression changes in RPT with cancer stem cell markers were highly significant. For example, aldehyde dehydrogenases 1A1 and 3A1 (ALDH1A1 and ALDH3A1), which are members of the human aldehyde dehydrogenase superfamily, constitute novel candidate cancer stem cell markers in various solid tumors in the testis, brain, lens, liver, lung and retina (27). These cytoplasmic enzymes act during the oxidative stress response (28), differentiation (29) and drug resistance (30). ALDH1A1 has been reported as a novel marker for glioblastoma cells with stem cell characteristics (31) and showed the highest level change (72.18-fold

higher in RPT than in NRPT) in the present study. The cancer stem cell marker CD24 was also differentially expressed (5.5-fold higher in RPT than in NRPT). In contrast to the finding on RPT and NRPT, expression of cancer stem cell markers, such as ALDH1A1, ALDH3A1, CD24, CXCL1 and IL-6 was mostly downregulated in metastatic lung nodules after γ-IR compared to RPT (Fig. 4).

Discussion

In the present study, we observed distant metastasis after local γ-IR using BLI of fLuc gene expressing rat glioma and [^{18}F]FLT and [^{18}F]FDG-PET. Next, we observed that γ-IR, particularly fractionated local γ-IR, increased stem cell marker expression in γ-IR primary tumors by microarray. We used the γ-IR dose and schedule for C6-L tumor-bearing mice as described by Camphausen *et al* (32), who used Lewis lung carcinoma cells to confirm that γ-IR promotes metastasis in a mouse model.

BLI has relatively low cost and high throughput capability, but the depth dependence of the signal is a major disadvantage in small animals. The other major limitation is that BLI does not provide anatomical information. Therefore, metastatic tumors in lung and spleen after γ-IR were confirmed by small-animal PET/CT. [^{18}F]FDG is the most widely used PET tracer and is indispensable for diagnosing and staging PET tracer for a variety of cancers. Several research groups have suggested that [^{18}F]FLT is useful as a PET tracer to monitor proliferation and other biological response of tumors to chemotherapy and radiotherapy (33-36).

In the present study, we evaluated [^{18}F]FDG and [^{18}F] FLT-PET as a potential diagnostic tool for monitoring the response to metastatic tumors after γ-IR in a tumor-bearing mouse model. We found high uptake of [^{18}F]FLT and [^{18}F] FDG in metastatic lung nodules after γ-IR. The four nodules that were discriminated by [^{18}F]FLT and [^{18}F]FDG-PET were detected as one spot on BLI (Fig. 2B). The other limitation of BLI is that it does not discriminate focal signals due to spill-over. Three metastatic lung nodules and one metastatic splenic nodule in another γ-IR C6-L bearing mouse were detected by [^{18}F]FLT-PET and autoradiography, but the splenic nodule was not detected by BLI due to a light penetration problem into deep tissue (Fig. 2C). Therefore, BLI and nuclear medicine imaging may be suitable for metastatic tumor screening after γ-IR and to more precisely locate metastatic tumors, respectively.

Recent studies have shown that a decreased cellular proliferation capacity is an early event in response to 20-Gy IR (37). We wondered whether proliferation had recovered in IR primary tumor lesions at 6 weeks γ-IR. Cancer stem cell markers were upregulated in γ-IR primary tumor lesions compared to that in non-IR primary tumors. We also found downregulation in a proportion of cancer stem cell markers in metastatic lung nodules. The proportion of cancer cell markers, particularly the ALDH family and CD24, increasing in γ-IR primary tumors may be important for distant metastasis in glioma. In particular, we revealed that upregulation of ALDH1A1 in γ-IR C6-L primary tumors may be a cancer stemness property. ALDH1A1 is a predominant isoform of the ALD family located in the cytoplasm (38) and has gained attention as a putative cancer stem cell and progenitor cell marker (39). Our data show that the small number of C6-L cells that survived in γ-IR C6-L primary tumors may have high ALDH1A1 expression, suggesting that cells surviving γ-IR are a source for distant metastasis. CD44 and CD90 have also been proposed as cancer stem-like cell markers in esophageal squamous cell carcinoma but cell heterogeneity limits their application (40,41).

We evaluated the metastatic tumors after γ-IR and found invasive/migration ability after local treatment of C6-L xenograft mice, suggesting that the small number of C6-L cells that survived in locally γ-IR treated tumors have more potential to metastasize, which is the main reason for recurrence of glioma after radiotherapy. The microarray study revealed more surviving cancer cells with cancer stem cell markers in the γ-IR primary tumors compared with those in the non-IR primary tumors. After formation of metastatic lung nodules in our experiments, expression of cancer stem cell markers may be downregulated as shown in our microarray data (Fig. 4). Recent studies in patients with glioma observed that the EMT may affect the ability of biomarkers to predict radio-resistant glioma (42). We observed downregulation of TGF-β and Smad5 and upregulation of MMPs, Fn1 and Snail2 in RPT compared with NRPT.

In summary, metastatic tumors were detected after fractionated γ-IR with ^{60}Co by non-invasive longitudinal imaging and repeated measurements of the metastatic tumors after γ-IR. We demonstrated that metastatic tumors after γ-IR are associated with several genes, including the EMT and enhanced cancer stem cell markers which result in cancer cell growth, survival, invasion and proliferation.

Acknowledgements

The present study was supported by the Korea Science and Engineering Foundation (KOSEF) grant funded by the Korea government (MEST) (NRF-2012M2A2A7013480).

References

1. Dirks PB: Brain tumor stem cells: Bringing order to the chaos of brain cancer. J Clin Oncol 26: 2916-2924, 2008.
2. Lawrence TS, Haffty BG and Harris JR: Milestones in the use of combined-modality radiation therapy and chemotherapy. J Clin Oncol 32: 1173-1179, 2014.
3. Govindan R, Bogart J and Vokes EE: Locally advanced non-small cell lung cancer: The past, present, and future. J Thorac Oncol 3: 917-928, 2008.
4. Cognetti DM, Weber RS and Lai SY: Head and neck cancer: An evolving treatment paradigm. Cancer 113 (Suppl): 1911-1932, 2008.
5. Gold KA, Lee HY and Kim ES: Targeted therapies in squamous cell carcinoma of the head and neck. Cancer 115: 922-935, 2009.
6. Stupp R, Mason WP, van den Bent MJ, Weller M, Fisher B, Taphoorn MJ, Belanger K, Brandes AA, Marosi C, Bogdahn U, *et al*; European Organisation for Research and Treatment of Cancer Brain Tumor and Radiotherapy Groups; National Cancer Institute of Canada Clinical Trials Group: Radiotherapy plus concomitant and adjuvant temozolomide for glioblastoma. N Engl J Med 352: 987-996, 2005.
7. Eifel PJ, Winter K, Morris M, Levenback C, Grigsby PW, Cooper J, Rotman M, Gershenson D and Mutch DG: Pelvic irradiation with concurrent chemotherapy versus pelvic and para-aortic irradiation for high-risk cervical cancer: An update of radiation therapy oncology group trial (RTOG) 90-01. J Clin Oncol 22: 872-880, 2004.

8. Baskar R, Lee KA, Yeo R and Yeoh KW: Cancer and radiation therapy: Current advances and future directions. Int J Med Sci 9: 193-199, 2012.
9. Prasanna A, Ahmed MM, Mohiuddin M and Coleman CN: Exploiting sensitization windows of opportunity in hyper and hypo-fractionated radiation therapy. J Thorac Dis 6: 287-302, 2014.
10. Suit HD: Local control and patient survival. Int J Radiat Oncol Biol Phys 23: 653-660, 1992.
11. Balasubramaniam A, Shannon P, Hodaie M, Laperriere N, Michaels H and Guha A: Glioblastoma multiforme after stereotactic radiotherapy for acoustic neuroma: Case report and review of the literature. Neuro Oncol 9: 447-453, 2007.
12. Kaplan HS and Murphy ED: The effect of local roentgen irradiation on the biological behavior of a transplantable mouse carcinoma; increased frequency of pulmonary metastasis. J Natl Cancer Inst 9: 407-413, 1949.
13. von Essen CF: Radiation enhancement of metastasis: A review. Clin Exp Metastasis 9: 77-104, 1991.
14. Núñez MI, McMillan TJ, Valenzuela MT, Ruiz de Almodóvar JM and Pedraza V: Relationship between DNA damage, rejoining and cell killing by radiation in mammalian cells. Radiother Oncol 39: 155-165, 1996.
15. Barcellos-Hoff MH, Park C and Wright EG: Radiation and the microenvironment - tumorigenesis and therapy. Nat Rev Cancer 5: 867-875, 2005.
16. Moulder JE and Rockwell S: Hypoxic fractions of solid tumors: Experimental techniques, methods of analysis, and a survey of existing data. Int J Radiat Oncol Biol Phys 10: 695-712, 1984.
17. Ghisolfi L, Keates AC, Hu X, Lee DK and Li CJ: Ionizing radiation induces stemness in cancer cells. PLoS One 7: e43628, 2012.
18. Zhou YC, Liu JY, Li J, Zhang J, Xu YQ, Zhang HW, Qiu LB, Ding GR, Su XM, Mei-Shi, *et al*: Ionizing radiation promotes migration and invasion of cancer cells through transforming growth factor-beta-mediated epithelial-mesenchymal transition. Int J Radiat Oncol Biol Phys 81: 1530-1537, 2011.
19. Gomez-Casal R, Bhattacharya C, Ganesh N, Bailey L, Basse P, Gibson M, Epperly M and Levina V: Non-small cell lung cancer cells survived ionizing radiation treatment display cancer stem cell and epithelial-mesenchymal transition phenotypes. Mol Cancer 12: 94, 2013.
20. Adseshaiah PP, Patel NL, Ileva LV, Kalen JD, Haines DC and McNeil SE: Longitudinal imaging of cancer cell metastases in two preclinical models: A correlation of noninvasive imaging to histopathology. Int J Mol Imaging 102702: 2014, 2014.
21. Kang JH and Chung JK: Molecular-genetic imaging based on reporter gene expression. J Nucl Med 49 (Suppl 2): 164S-179S, 2008.
22. Park JH, Kim KI, Lee YJ, Lee TS, Kim KM, Nahm SS, Park YS, Cheon GJ, Lim SM and Kang JH: Non-invasive monitoring of hepatocellular carcinoma in transgenic mouse with bioluminescent imaging. Cancer Lett 310: 53-60, 2011.
23. Kim KI, Park JH, Lee YJ, Lee TS, Park JJ, Song I, Nahm SS, Cheon GJ, Lim SM, Chung JK, *et al*: In vivo bioluminescent imaging of α-fetoprotein-producing hepatocellular carcinoma in the diethylnitrosamine-treated mouse using recombinant adenoviral vector. J Gene Med 14: 513-520, 2012.
24. Park JH, Kang JH, Lee YJ, Kim KI, Lee TS, Kim KM, Park JA, Ko YO, Yu DY, Nahm SS, *et al*: Evaluation of diethylnitrosamine- or hepatitis B virus X gene-induced hepatocellular carcinoma with ^{18}F-FDG PET/CT: A preclinical study. Oncol Rep 33: 347-353, 2015.
25. Gown AM: Current issues in ER and HER2 testing by IHC in breast cancer. Mod Pathol 21 (Suppl 2): S8-S15, 2008.
26. Park JK, Jang SJ, Kang SW, Park S, Hwang SG, Kim WJ, Kang JH and Um HD: Establishment of animal model for the analysis of cancer cell metastasis during radiotherapy. Radiat Oncol 7: 153-163, 2012.
27. Vasiliou V, Thompson DC, Smith C, Fujita M and Chen Y: Aldehyde dehydrogenases: From eye crystallins to metabolic disease and cancer stem cells. Chem Biol Interact 202: 2-10, 2013.
28. Marchitti SA, Brocker C, Stagos D and Vasiliou V: Non-P450 aldehyde oxidizing enzymes: The aldehyde dehydrogenase superfamily. Expert Opin Drug Metab Toxicol 4: 697-720, 2008.
29. Chute JP, Muramoto GG, Whitesides J, Colvin M, Safi R, Chao NJ and McDonnell DP: Inhibition of aldehyde dehydrogenase and retinoid signaling induces the expansion of human hematopoietic stem cells. Proc Natl Acad Sci USA 103: 11707-11712, 2006.
30. Muramoto GG, Russell JL, Safi R, Salter AB, Himburg HA, Daher P, Meadows SK, Doan P, Storms RW, Chao NJ, *et al*: Inhibition of aldehyde dehydrogenase expands hematopoietic stem cells with radioprotective capacity. Stem Cells 28: 523-534, 2010.
31. Rasper M, Schäfer A, Piontek G, Teufel J, Brockhoff G, Ringel F, Heindl S, Zimmer C and Schlegel J: Aldehyde dehydrogenase 1 positive glioblastoma cells show brain tumor stem cell capacity. Neuro Oncol 12: 1024-1033, 2010.
32. Camphausen K, Moses MA, Beecken WD, Khan MK, Folkman J and O'Reilly MS: Radiation therapy to a primary tumor accelerates metastatic growth in mice. Cancer Res 61: 2207-2211, 2001.
33. Murayama C, Harada N, Kakiuchi T, Fukumoto D, Kamijo A, Kawaguchi AT and Tsukada H: Evaluation of D-^{18}F-FMT, ^{18}F-FDG, L-11C-MET, and ^{18}F-FLT for monitoring the response of tumors to radiotherapy in mice. J Nucl Med 50: 290-295, 2009.
34. Molthoff CF, Klabbers BM, Berkhof J, Felten JT, van Gelder M, Windhorst AD, Slotman BJ and Lammertsma AA: Monitoring response to radiotherapy in human squamous cell cancer bearing nude mice: comparison of 2'-deoxy-2'-[^{18}F]fluoro-D-glucose (FDG) and 3'-[^{18}F]fluoro-3'-deoxythymidine (FLT). Mol Imaging Biol 9: 340-347, 2007.
35. Yang YJ, Ryu JS, Kim SY, Oh SJ, Im KC, Lee H, Lee SW, Cho KJ, Cheon GJ and Moon DH: Use of 3'-deoxy-3'-[^{18}F]fluorothymidine PET to monitor early responses to radiation therapy in murine SCCVII tumors. Eur J Nucl Med Mol Imaging 33: 412-419, 2006.
36. Sugiyama M, Sakahara H, Sato K, Harada N, Fukumoto D, Kakiuchi T, Hirano T, Kohno E and Tsukada H: Evaluation of 3'-deoxy-3'-^{18}F-fluorothymidine for monitoring tumor response to radiotherapy and photodynamic therapy in mice. J Nucl Med 45: 1754-1758, 2004.
37. Wang H, Liu B, Tian J, Xu B, Zhang J, Qu B and Chen Y: Evaluation of ^{18}F-FDG and ^{18}F-FLT for monitoring therapeutic responses of colorectal cancer cells to radiotherapy. Eur J Radiol 82: e484-e491, 2013.
38. Hess DA, Craft TP, Wirthlin L, Hohm S, Zhou P, Eades WC, Creer MH, Sands MS and Nolta JA: Widespread nonhematopoietic tissue distribution by transplanted human progenitor cells with high aldehyde dehydrogenase activity. Stem Cells 26: 611-620, 2008.
39. Douville J, Beaulieu R and Balicki D: ALDH1 as a functional marker of cancer stem and progenitor cells. Stem Cells Dev 18: 17-25, 2009.
40. Zhao JS, Li WJ, Ge D, Zhang PJ, Li JJ, Lu CL, Ji XD, Guan DX, Gao H, Xu LY, *et al*: Tumor initiating cells in esophageal squamous cell carcinomas express high levels of CD44. PLoS One 6: e21419, 2011.
41. Zhao R, Quaroni L and Casson AG: Identification and characterization of stemlike cells in human esophageal adenocarcinoma and normal epithelial cell lines. J Thorac Cardiovasc Surg 144: 1192-1199, 2012.
42. Meng J, Li P, Zhang Q, Yang Z and Fu S: A radiosensitivity gene signature in predicting glioma prognostic via EMT pathway. Oncotarget 5: 4683-4693, 2014.